In Situ Transmission Electron Microscopy to Study the Location and Distribution Effect of Pt on the Reduction of Co$_3$O$_4$–SiO$_2$

*Min Tang, Petra E. de Jongh, and Krijn P. de Jong**

The addition of Pt generally promotes the reduction of Co$_3$O$_4$ in supported catalysts, which further improves their activity and selectivity. However, due to the limited spatial resolution, how Pt and its location and distribution affect the reduction of Co$_3$O$_4$ remains unclear. Using ex situ and in situ ambient pressure scanning transmission electron microscopy, combined with temperature-programmed reduction, the reduction of silica-supported Co$_3$O$_4$ without Pt and with different location and distribution of Pt is studied. Shrinkage of Co$_3$O$_4$ nanoparticles is directly observed during their reduction, and Pt greatly lowers the reduction temperature. For the first time, the initial reduction of Co$_3$O$_4$ with and without Pt is studied at the nanoscale. The initial reduction of Co$_3$O$_4$ changes from surface to interface between Co$_3$O$_4$ and SiO$_2$. Small Pt nanoparticles located at the interface between Co$_3$O$_4$ and SiO$_2$ promote the reduction of Co$_3$O$_4$ by the detachment of Co$_3$O$_4$/CoO from SiO$_2$. After reduction, the Pt and part of the Co form an alloy with Pt well dispersed. This study for the first time unravels the effects of Pt location and distribution on the reduction of Co$_3$O$_4$ nanoparticles, and helps to design cobalt-based catalysts with efficient use of Pt as a reduction promoter.

1. Introduction

Supported non-noble metal catalysts, such as Fe, Co, and Ni, are often difficult to obtain or to keep in the metallic state.[1–5] The addition of noble metal promoters (e.g., Pt) facilitates the reduction of the non-noble metal oxide precursors, which greatly improves the performance of the catalysts.[6–9] For example, Co is widely used in Fischer–Tropsch synthesis (FTS),[10–12] and the addition of Pt generally enhances the degree of reduction of cobalt oxide or helps to stabilize smaller metallic Co nanoparticles (NPs) and hence accelerates the FTS rates.[13–18] It is commonly postulated that the improved reducibility upon addition of noble metal promoters occurs via hydrogen spillover from the promoter to the cobalt oxides.[9,19,20] Jacobs et al. reported that the isolated Pt atoms interact with supported cobalt clusters without forming observable Pt—Pt bonds by using in situ extended X-ray absorption fine structure.[20] They thought that these Pt atoms must be in intimate contact with the Co clusters to account for a spillover mechanism.[20] Nabaho et al. demonstrated the spillover mechanism in physical mixed hybrid catalysts (Pt/Al$_2$O$_3$ and Co/Al$_2$O$_3$) despite physical separation of Pt from Co.[19] Due to the limited spatial resolution, the location and distribution of Pt are not clarified in most of the studies.[17,22] How exactly the Pt and its location and distribution affect the reduction of Co$_3$O$_4$ remains unclear. For example, should Pt be located on the support or on the Co$_3$O$_4$ nanoparticles? Are Pt nanoparticles more effective than Pt clusters or single atoms?

Transmission electron microscopy (TEM), with high spatial resolution, is an established technology to visualize the location and distribution of Pt in Pt—Co$_3$O$_4$ precursors.[21] With an in situ gas holder or an environmental transmission electron microscope (ETEM),[23–26] we can now monitor the reduction process of Co$_3$O$_4$ at atomic scale.[27–34] By using the in situ gas holder in a Cs aberration-corrected microscope, Dembélé et al. monitored the fragmentation of cobalt aggregates, the disappearance of cavities within the particles, their shape changes, the particle diffusion, and coalescence processes, on the behavior of the Co phase of Pt—Co$_3$O$_4$/SiO$_2$. However, they did not clarify the location and distribution of Pt and its effect on the reduction of Co$_3$O$_4$.[31] Dehghan et al. studied the reduction of 12 wt% Co/0.5 wt% Re/a-Al$_2$O$_3$ in an ETEM.[34] They found that the original Co$_3$O$_4$ aggregates tended to fall apart enhancing the active surface area during the reduction; however, no differences of the reduction behavior between the promoted and nonpromoted catalysts were observed.

Herein, through ex situ atomic resolution high angle annular dark-field scanning transmission electron microscopy

M. Tang, P. E. de Jongh, K. P. de Jong
Materials Chemistry and Catalysis
Debye Institute for Nanomaterials Science
Utrecht University
Utrecht 3584 CG, The Netherlands
E-mail: K.P.deJong@uu.nl

ADVANCED
SCIENCE NEWS

www.advancedsciencenews.com

NANO · MICRO

small

www.small-journal.com

(HAADF-STEM), the location and distribution of Pt are clarified for different Pt-promoted Co_3O_4 precursors. By using in situ ambient pressure STEM, we directly visualize the reduction process of Co_3O_4. Shrinkage of Co_3O_4 NPs was observed during the reduction. We found that Pt greatly lowered the reduction temperature and changed the initiation of Co_3O_4 reduction. Pt and Co formed alloyed NP during the reduction and separated from the pure Co part. Interestingly, Pt at the interface between Co_3O_4 and SiO_2 promoted the reduction of CoO to Co stronger compared with the Pt single atoms or clusters inside the Co_3O_4 crystals. These in situ STEM results explained well the different temperature-programmed reduction (TPR) peaks of the three precursors studied.

2. Results and Discussion

2.1. Fresh Precursors' Characterization

Three catalyst precursors, without Pt and with different location and distribution of Pt, were synthesized using a wet impregnation method, i.e., Co_3O_4—SiO_2 with 4.8 wt% Co without Pt, Pt—Co_3O_4—SiO_2-co with 4.8 wt% Co and 1.0 wt% Pt via co-impregnation, and Pt—Co_3O_4—SiO_2-se with 4.8 wt% Co and 1.0 wt% Pt via sequential impregnation. Co-impregnation, adding Co precursor and Pt precursor together, may result in well-mixed Co_3O_4 and Pt. For sequential impregnation, adding Pt precursor to the prepared Co_3O_4—SiO_2 precursor could result in separate Co_3O_4 and Pt. More details about synthesis are shown in the Supporting Information.

X-ray diffraction (XRD) was used to examine the crystal structure and phase purity of the calcined precursors. **Figure 1** shows the wide-angle XRD patterns of the three kinds of precursors, Co_3O_4—SiO_2, Pt—Co_3O_4—SiO_2-co, and Pt—Co_3O_4—SiO_2-se, with
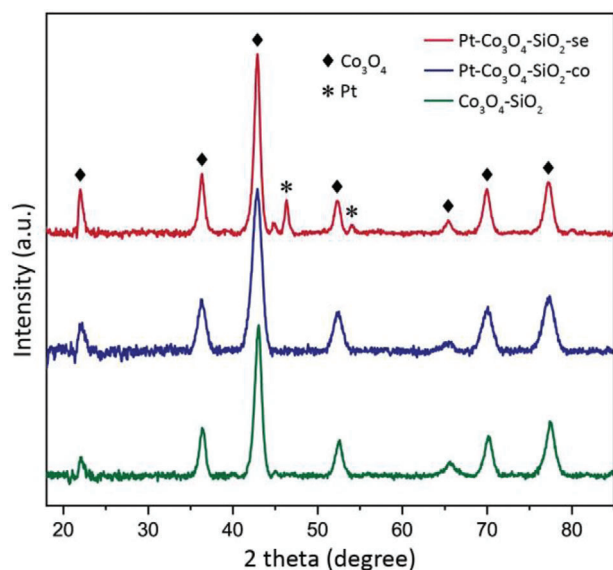
Figure 1. XRD patterns of as-prepared three kinds of precursors, Co_3O_4–SiO_2, Pt–Co_3O_4–SiO_2-co, and Pt–Co_3O_4–SiO_2-se, with baseline and support OX-50 subtracted. Indexing is based on $a = 0.8084$ nm ($Fd3m$) for Co_3O_4, and $a = 0.3923$ nm ($Fm3m$) for Pt. The original patterns are shown in Figure S1 (Supporting Information).

the baseline and support material OX-50 being subtracted. The diffraction peaks marked by black rhombus identify the precursors as cubic Co_3O_4 ($a = 0.8084$ nm, $Fd3m$, Powder Diffraction File Database (PDF-2) entry: 42–1467) for all these three precursors. The average crystallite sizes of Co_3O_4 roughly estimated on the basis of the Scherrer formula are 9.4, 7.5, and 10.7 nm for Co_3O_4—SiO_2, Pt—Co_3O_4—SiO_2-co, and Pt—Co_3O_4—SiO_2-se, respectively. The diffraction peaks marked by asterisk of Pt—Co_3O_4—SiO_2-se are identified as Pt (111) and Pt (200) ($a = 0.3923$ nm, $Fm3m$, PDF-2 entry: 04–0802). However, no Pt diffraction peaks were observed in the pattern of Pt—Co_3O_4—SiO_2-co.

The morphology and size of the three kinds of precursors were measured by HAADF-STEM. As shown in **Figure 2**a–c, the Co_3O_4 NPs were distributed over OX-50 quite nonuniformly for all these three precursors as is expected for the synthesis route applied. The particle size distribution of Co_3O_4 is acquired from more than 200 NPs. The mean sizes of Co_3O_4 were 9.5, 8.0, and 11.6 nm for Co_3O_4—SiO_2, Pt—Co_3O_4—SiO_2-co, and Pt—Co_3O_4—SiO_2-se, respectively. The sizes are close to the values obtained from XRD results. The Pt-promoted co-impregnation sample had the slightly lower size, possibly because of the Pt-precursor. The sequential impregnation sample displayed the largest sizes, possibly due to some Ostwald ripening of Co_3O_4 during the second impregnation step. Except the small variation of particle sizes, there are no big differences for these three samples from the low-magnification HAADF-STEM images, which is a good starting point to study the effects of Pt on the reducibility of Co_3O_4.

To further study the location and distribution of Pt, the atomic resolution HAADF-STEM images were acquired for these three precursors (Figure 2d–f). The lattice spacings are 2.431, 2.827, and 2.817 Å for the NPs in Figure 2d,e, which corresponds to Co_3O_4 (311), (220), and (220), respectively. These results demonstrated that the supported NPs in all these three precursors were Co_3O_4. For Pt-promoted samples, except the big Co_3O_4 NPs, there were many bright dots and clusters (marked by blue dashed circles), and small NPs (marked by yellow dashed circles) which could be Pt, as shown in Figure 2e,f. The energy-dispersive X-ray spectroscopy (EDS) elemental mapping further demonstrated that as shown in Figures S2 and S3 (Supporting Information). It is worth noting that although Pt single atoms, clusters, and NPs are everywhere, the Pt was mainly located inside or on the surface of the Co_3O_4 crystals as Pt single atoms or clusters for Pt—Co_3O_4—SiO_2-co (Figure 2e). For Pt—Co_3O_4—SiO_2-se, there were more Pt NPs located at the interface between Co_3O_4 and SiO_2 (Figure 2f). More examples are shown in Figures S4 and S5 (Supporting Information).

X-ray photoelectron spectroscopy (XPS) results show that the surface of the sequentially prepared sample contains much more Pt than the surface of the co-impregnated sample as shown by a much higher Pt/(Si+O) ratio for the sequential impregnated sample (see **Table 1**). These results agreed well with the STEM results in Figure 2e,f that Pt located mainly inside the Co_3O_4 crystals for Pt—Co_3O_4—SiO_2-co, while at the interface between Co_3O_4 and SiO_2 for Pt—Co_3O_4—SiO_2-se. The XPS results also show that the particle size of Co_3O_4 for sequential impregnated sample is bigger than for the co-impregnated sample as shown by a lower Co/(Si+O) ratio
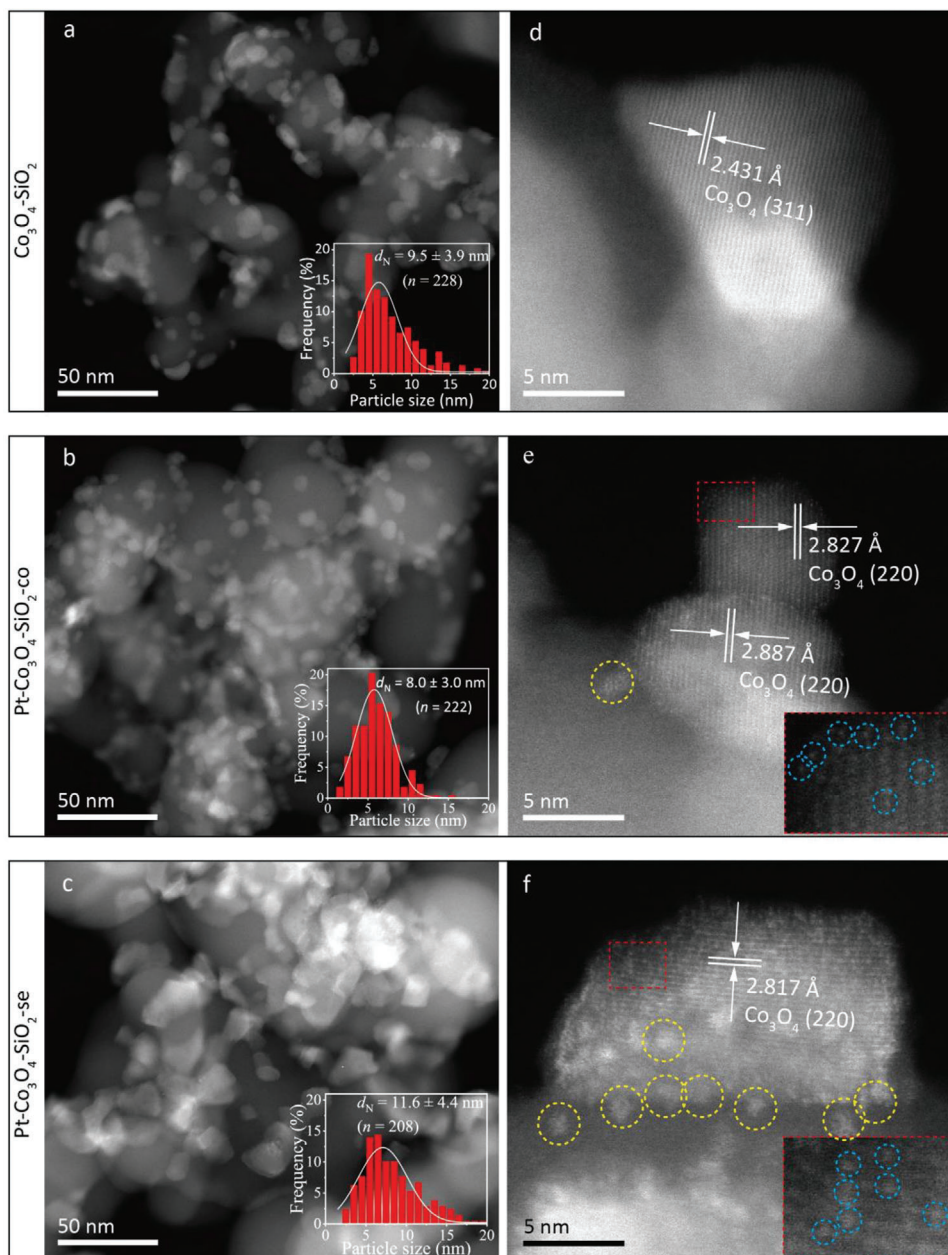
ADVANCED
SCIENCE NEWS

www.advancedsciencenews.com

NANO · MICRO

small

www.small-journal.com

Figure 2. a–c) HAADF-STEM images showing the morphology and size of the three precursors. The particle size distribution of Co_3O_4, obtained from more than 200 NPs, is inserted in each image. d–f) Atomic resolution HAADF-STEM images showing the lattice spacing of Co_3O_4 and the Pt distribution marked by yellow (Pt NPs) and blue (Pt clusters and single atoms) dashed circles. The inset images in panels (e) and (f) are the corresponding magnified area marked by a red dashed rectangle.

Table 1. X-ray photoelectron spectroscopy (XPS) results showing the surface ratio of (Co+Pt) to (Si+O) and Pt to Co for the two precursors with Pt.

	co-impregnation		se-impregnation	
	Position 1	Position 2	Position 1	Position 2
Co/(Si+O) at. ratio ×100	0.58	0.49	0.37	0.33
Pt/(Si+O) at. ratio ×100	0.09	0.08	0.16	0.16

for the sequentially impregnated sample (see Table 1), which agreed well with XRD and STEM results. The Pt 4f and Co 2p photoelectron spectra are shown in Figure S6 (Supporting Information).

2.2. The Reducibility of the Precursors (TPR)

The reducibility of the precursors after calcination characterized by TPR is shown in **Figure 3**. The TPR profile of Co_3O_4—SiO_2
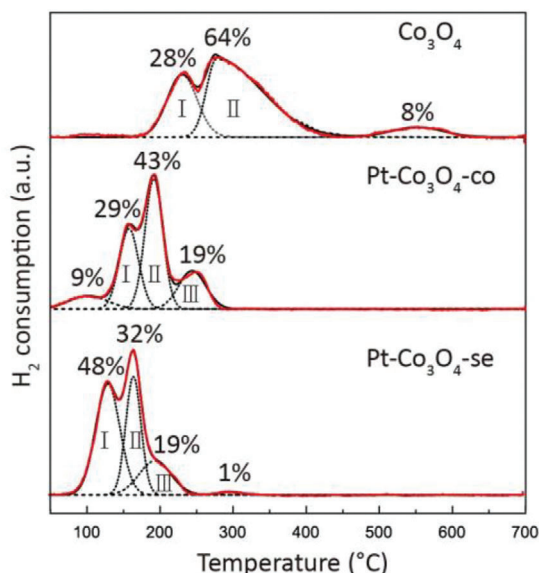
ADVANCED
SCIENCE NEWS

www.advancedsciencenews.com

NANO · MICRO

small

www.small-journal.com

Figure 3. TPR profiles of Co_3O_4–SiO_2, Pt–Co_3O_4–SiO_2-co, and Pt–Co_3O_4–SiO_2-se precursors.

reveals two major peaks, which are attributed to the successive reduction of Co^{3+} to Co^{2+}, $Co_3O_4 + H_2 = 3CoO + H_2O$, and further to Co^0, $3CoO + 3H_2 = 3Co + 3H_2O$[9,20,35] in the temperature range of 180–400 °C. The expected ratio of the peak areas is equal to the ratio of the calculated H_2 consumption, which is 1:3. The small peak at high temperature (about 550 °C) is the reduction of cobalt silicate complexes which likely formed during the reduction at high temperature. The area of the second peak II (64%) plus the cobalt silicate peak (8%) is about 2.6 times to the first one I (28%). The Pt-promoted precursors were reduced at much lower temperatures for both reduction steps (Co_3O_4 to CoO and CoO to Co), in the range of 100–300 °C (Pt—Co_3O_4—SiO_2-co) and 80–250 °C (Pt—Co_3O_4—SiO_2-se). The shapes of the major peaks were different indicating different reduction processes, which is due to the presence and different location and distribution of Pt as shown in Figure 2e,f. For both Pt-promoted precursors, the area of the second peak II is no longer three times to the first peak I, even peak II plus peak III is far less than three times of peak I, so peak I must contain some direct reduction processes, from Co_3O_4 to Co, especially for Pt—Co_3O_4—SiO_2-se. The first small peak (9%) for the co-impregnated sample might be the reduction of PtO or cobalt salts. The fourth peak (1%) for the sequential impregnation sample may be the reduction of Co_3O_4 NPs without Pt since the reduction temperature is similar to the sample without Pt. There were two separate peaks, II and III, corresponding to the reduction of CoO to Co following peak I, indicating that there were at least two different Co_3O_4 crystals promoted by Pt differently. In addition, the TPR profile of Pt promoted precursors did not show the peak of the reduction for cobalt silicates, which suggested that these species formed during the TPR analysis rather than during catalyst preparation. The above TPR results indicated the different reducibility of these three precursors and significant effects of Pt on the reduction process of Co_3O_4.

2.3. In Situ STEM to Study the Reduction of the Three Precursors

To investigate the process of Co_3O_4 reduction and the effect of Pt at the nanoscale, in situ ambient pressure STEM was employed. In order to study the electron beam effects, several regions were observed with different accumulated electron dose for each precursor as shown in Figure S7 (Supporting Information). For the Co_3O_4—SiO_2 precursor, shrinkage of the individual cobalt oxide NPs was observed after reduction at 400 °C in 5% H_2/Ar (**Figure 4**a,b). Aggregates of Co_3O_4 NPs with brighter contrast at the center (Figure 4a, number 7, and Figure 4c) were reduced to two Co NPs (Figure 4b, number 7, and Figure 4d); one small single crystal Co_3O_4 NP (Figure 4a, number 8, and Figure 4e) was reduced to one Co NP (Figure 4b, number 8, and Figure 4f). To get more details during the reduction, we performed in situ reduction at a range of temperatures, from 25 to 400 °C (Figure 4g–p). At 100 °C, no obvious change was observed (Figure 4h,m). At 200 °C, some bright contrast on the surface of NP indicated that the reduction from Co^{3+} to Co^{2+} started from the surface of Co_3O_4 (Figure 4i,n). More examples are shown in Figures S8 and S9 (Supporting Information). When further increased the temperature to 300 °C, the bright contrast part became bigger (Figure 4j,o). At 400 °C, the NPs further shrank and redispersed to several small NPs (Figure 4k,p).

For the Pt-promoted precursors, the in situ STEM results are shown in **Figure 5**, at room temperature in Ar (Figure 5a,g) and directly after reduction at 400 °C in 5% H_2/Ar (Figure 5b,h). Besides the obvious shrinkage similar to samples without Pt, the aggregate Pt NPs sintered. After reduction, for the co-impregnated sample, the Co_3O_4 NP changed to separate parts with bright contrast and weak contrast (Figure 5d,f). For the sequential impregnation sample, the bright particle was always surrounded by some parts with weaker contrast (Figure 5j,l). Another big difference for these two Pt-promoted precursors is that the Pt sintered strongly for the sequential impregnation sample, which is probably due to the small Pt NPs and its location on the surface but not inside the Co_3O_4 NPs. However, at such low magnification, from the morphology and the contrast of the NPs, we have limited information about the distribution of Pt after reduction.

To study the reduction process of Pt-promoted precursors in detail, the whole reduction was imaged over a range of temperatures. At 100 °C, there were already some changes, with dark contrast appearing at the interface, marked by red arrows in **Figure 6**g,q, which indicates that part of the NP detached from the SiO_2 support due to its shrinkage after the reduction. And there was no brighter contrast on the surface of the NP. These results demonstrated that the reduction started from the interface between Co_3O_4 and SiO_2. More examples are seen in Figures S10–S13 (Supporting Information). Interestingly, the initiation of reduction is always with Pt nanoparticles' aside. At 200 °C, obvious shrinkage was observed (Figure 6h,r). At 300 °C, for the co-impregnated one, the NP continued to shrink (Figure 6i), while for the sequential impregnated sample, the NP split, i.e., two parts appeared, the part with bright contrast and another part with weak contrast. The part in direct contact with Pt may sinter together with Pt forming an alloy, the part not in intimate contact with Pt detached from the support (Figure 6s). It seems that only Pt nanoparticles at the interface between Co_3O_4 and SiO_2 lead to detachment of Co from the SiO_2
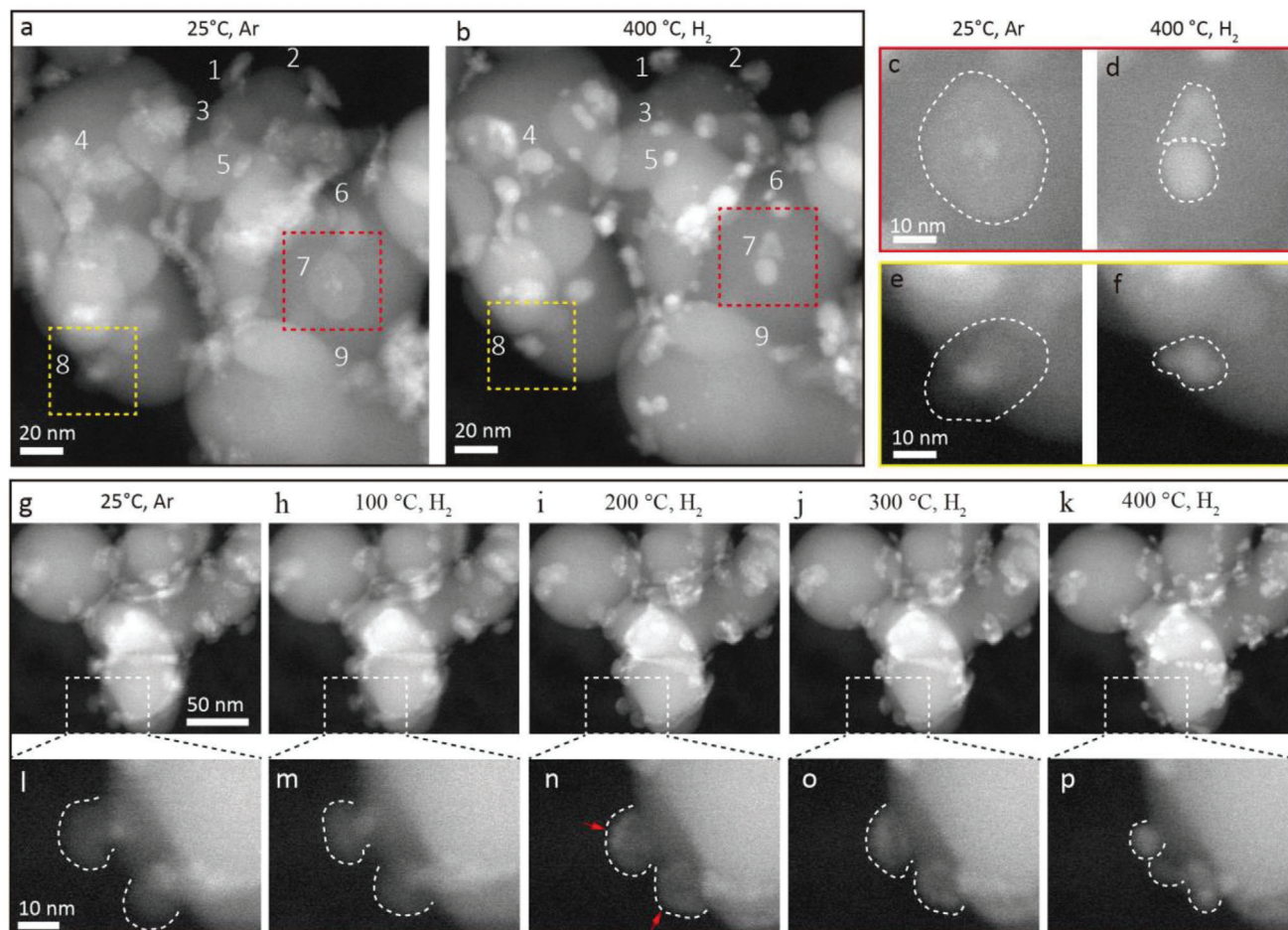
2304683 (4 of 9)

**ADVANCED
SCIENCE NEWS**

www.advancedsciencenews.com

**NANO · MICRO
small**

www.small-journal.com

Figure 4. a,b) In situ HAADF-STEM images for direct reduction of Co_3O_4–SiO_2 in 1 bar 5%H_2/Ar a) from room temperature to b) 400 °C. c–f) Magnified images for NPs c,d) numbered 7 and e,f) 8 in panels (a) and (b). g–p) In situ STEM results showing the reduction process of Co_3O_4 in 1 bar 5%H_2/Ar at a range of temperatures, g–k) from 25 to 400 °C and l–p) corresponding zooming area marked by white dashed rectangles. The accumulated electron dose $D = 9252\ e^-\ Å^{-2}$.

support. At 400 °C, the co-impregnated sample was reduced to NPs with Pt and Co together (Figure 6j), while the sequentially impregnated one displayed weak contrast parts surrounding the bright contrast part (Figure 6t). Different regions with a series of accumulated electron dose gave similar results, as shown in Figures S14–S21 (Supporting Information), which indicated that our in situ STEM results were not affected by the electron beam.

2.4. Ex Situ STEM to Identify the Distribution of Pt After Reduction

To study the Pt distribution after reduction, the chips used in in situ STEM experiments were observed using an inspection holder in a double Cs-corrected microscope. **Figure 7**a–f shows the EDS elemental mapping for Pt—Co_3O_4-co (Figure 7a–c) and Pt—Co_3O_4-se (Figure 7d–f), respectively. The bright NPs in HAADF-STEM images (Figure 7a,d) contained Co and Pt (Figure 7b,c,e,f) which indicated that the bright NPs were alloyed. The NPs with weaker contrast near (Figure 7a) or surrounding

(Figure 7d) the bright NPs were Co (Figure 7b,e). Figure 7g,h shows atomic resolution HAADF-STEM images for Pt—Co_3O_4-co (Figure 7g) and Pt—Co_3O_4-se (Figure 7h), respectively. The lattice spacing of the bright NPs corresponding to CoO as the reduced samples was passivated in air. These results showed that the Pt did not sinter to Pt NPs, but instead formed alloy with Co after reduction. We also did ex situ reduction in a quartz reactor to compare with in situ reduction for these three precursors. Because of the passivation in less than 0.1 ppm H_2O and O_2, the Co NPs were re-oxidized and encapsulated by a CoO/Co_3O_4 shell as shown in atomic resolution HAADF-STEM images (Figure 7i–k). More examples are shown in Figure S22 (Supporting Information). The statistical data for the shell size and the shell composition are shown in Figure S23 and S24 (Supporting Information), respectively. The Co_3O_4—SiO_2 sample showed the Co core and the averaged 2.8 nm CoO/Co_3O_4 shell. The precursors with Pt showed a smaller CoO/Co_3O_4 shell, 2.1 nm for Pt—Co_3O_4—SiO_2-co and 1.9 nm for Pt—Co_3O_4—SiO_2-se. The different Co/Co3O4 shell sizes indicate that the Pt not only promotes the reduction of Co_3O_4, but also hinders the reoxidation of Co. Pt cluster or single atoms were inside the reduced Co core and Pt NPs are outside
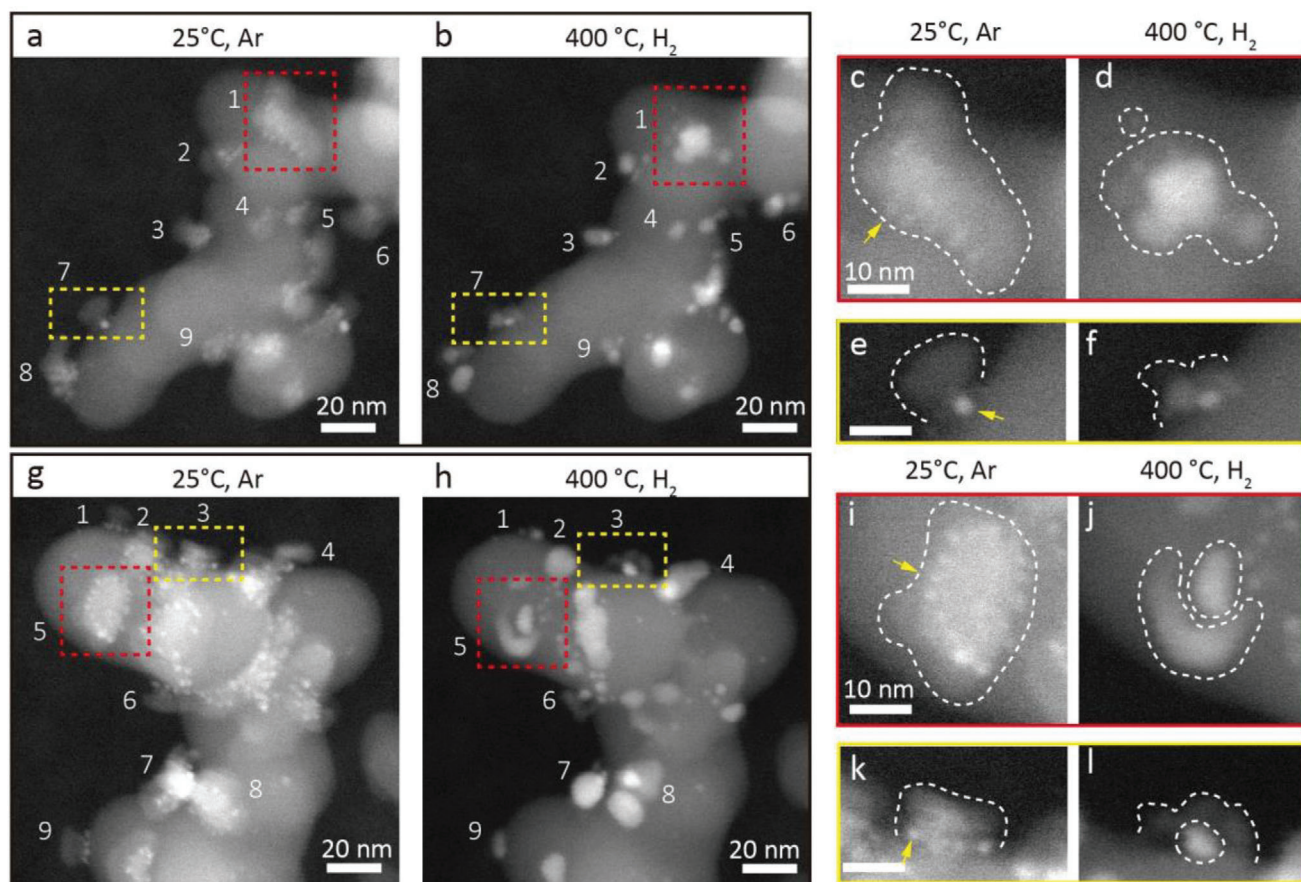
Figure 5. a,b) In situ HAADF-STEM images for direct reduction of Pt-Co$_3$O$_4$–SiO$_2$-co in 1 bar 5%H$_2$/Ar a) from room temperature to b) 400 °C. c–f) Magnified images of c,d) number 1 NP and e,f) number 7 NP in panels (a) and (b). g,h) In situ HAADF-STEM images for direct reduction of Pt–Co$_3$O$_4$-se in 1 bar 5%H$_2$/Ar from g) room temperature to h) 400 °C. i–l) Magnified images of i,j) number 5 NP and k,l) number 3 NP in panels (g) and (h).

the Co core, marked by yellow dashed circles (Figure 7j,k). These ex situ reduction results agreed well with in situ reduction results that Pt was distributed uniformly in Co after reduction. However, the reduced catalysts after passivation in ex situ reduction experiments (Figure 7j,k) were a little different from those in in situ STEM experiments (Figure 7g,h) because of different reduction condition, such as gas flow rate and hydrodynamics.

2.5. A Schematic Model for the Effects of Pt Promotion on the Reduction of Co$_3$O$_4$

A structural model was derived, as shown in **Figure 8**, to present the effects of Pt promotion and its location and distribution on the reduction of Co$_3$O$_4$ to Co. The location and distribution of Pt for the two Pt—Co$_3$O$_4$—SiO$_2$ precursors were different, i.e., the Pt was mainly located inside or on the surface of Co$_3$O$_4$ crystals as Pt single atoms or clusters for Pt—Co$_3$O$_4$—SiO$_2$-co, and at the interface between Co$_3$O$_4$ and SiO$_2$ as Pt NPs for Pt—Co$_3$O$_4$—SiO$_2$-se, demonstrated from the atomic resolution HAADF-STEM images (Figure 2) and XPS results (Table 1). The addition of Pt decreased the reduction temperature and changed the reduction

process significantly, as shown in TPR and in situ STEM results (Figures 3–6). Without Pt, the reduction of Co$_3$O$_4$ to CoO started from the surface of Co$_3$O$_4$, and further reduction of CoO to Co with limited but distinct formation of some cobalt silicates. The Pt affected the initiation of Co$_3$O$_4$ reduction from the surface of the NP to the interface between Co$_3$O$_4$ and SiO$_2$. Small Pt NPs supported at the interface between Co$_3$O$_4$ and SiO$_2$, led to detachment of Co$_3$O$_4$/CoO from the SiO$_2$ support due to the shrinkage of Co$_3$O$_4$ and the alloy formation of Pt and reduced Co (Figure 7), which weakened the metal oxide support interaction and promoted the reduction of CoO to Co strongly. Pt clusters or single atoms inside or on the surface of Co$_3$O$_4$ crystals did not weaken the metal oxide support interaction and mainly promoted the Co$_3$O$_4$ reduction via hydrogen dissociation. Therefore, the reduction temperature of Pt—Co$_3$O$_4$—SiO$_2$-co precursor was higher than that of Pt—Co$_3$O$_4$—SiO$_2$-se precursor. When the reduction was complete, the reduced Co NPs were detached from the SiO$_2$ support and surrounded the Pt$_x$Co$_y$ alloy for the Pt—Co$_3$O$_4$—SiO$_2$-se precursor. While for Pt—Co$_3$O$_4$—SiO$_2$-co precursor, the reduced Co NPs were located on the SiO$_2$ support with Pt$_x$Co$_y$ alloy nearby. In the presence of Pt, cobalt silicates were not formed.
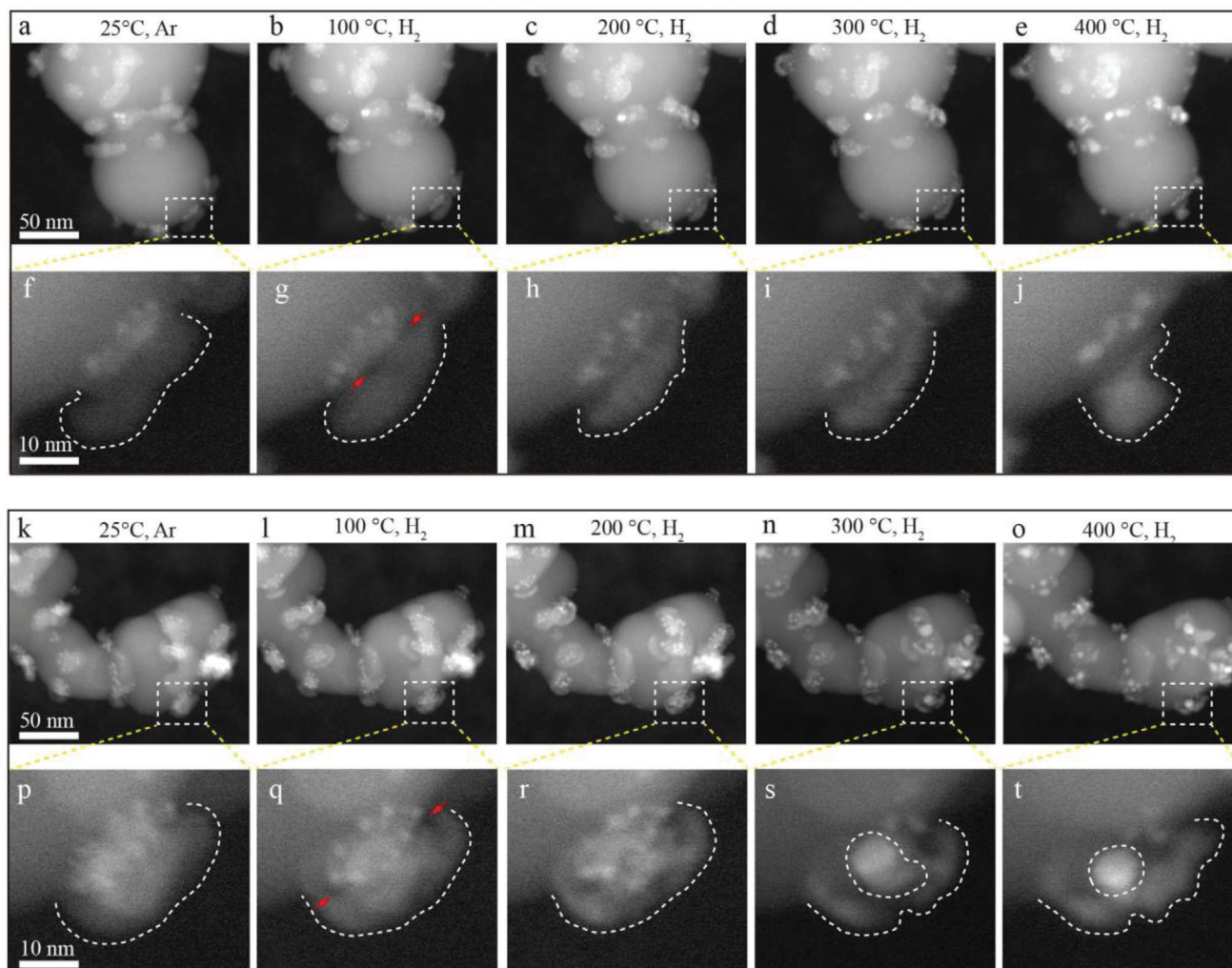
**ADVANCED
SCIENCE NEWS**

www.advancedsciencenews.com

NANO · MICRO

small

www.small-journal.com

Figure 6. a–j) In situ HAAFD-STEM results showing the reduction process of Pt-Co$_3$O$_4$-SiO$_2$-co in 1 bar 5%H$_2$/Ar over a range of temperatures, a–e) from 25 to 400 °C and f–j) corresponding zooming area marked by white dashed rectangles. The accumulated electron dose $D = 24\,200\ e^-$ Å^{-2}. k–t) In situ HAAFD-STEM results showing the reduction process of Pt-Co$_3$O$_4$-se in 1 bar 5%H$_2$/Ar at a range of temperatures, k–o) from 25 to 400 °C and p–t) corresponding zooming area marked by white dashed rectangles. The accumulated electron dose $D = 21234\ e^-$ Å^{-2}.

3. Conclusion

In conclusion, using aberration-corrected STEM, in situ ambient pressure STEM, and TPR, we studied the Pt promoting effect on the reduction of Co$_3$O$_4$ and clarified the significant role of the location and distribution of Pt. Shrinkage of Co$_3$O$_4$ NPs was observed during the reduction due to the removal of oxygen, the density differences between oxide and metal and the rounding off of metallic NP. Pt greatly lowered the reduction temperature and changed the reduction initiation of Co$_3$O$_4$ from its surface to the Co$_3$O$_4$ and SiO$_2$ interface. The Pt NPs at the interface between Co$_3$O$_4$ and SiO$_2$ promoted the reduction of Co$_3$O$_4$ stronger when compared with the Pt single atoms or clusters on the surface or inside the Co$_3$O$_4$ NPs. Pt distributed well and formed alloy with part of reduced Co after reduction. This work provides direct evidence of the effect of Pt location and distribution on the reduction of Co$_3$O$_4$ and gives a way for the rational design of efficient cobalt-based catalysts.

Supporting Information

Supporting Information is available from the Wiley Online Library or from the author.

Conflict of Interest

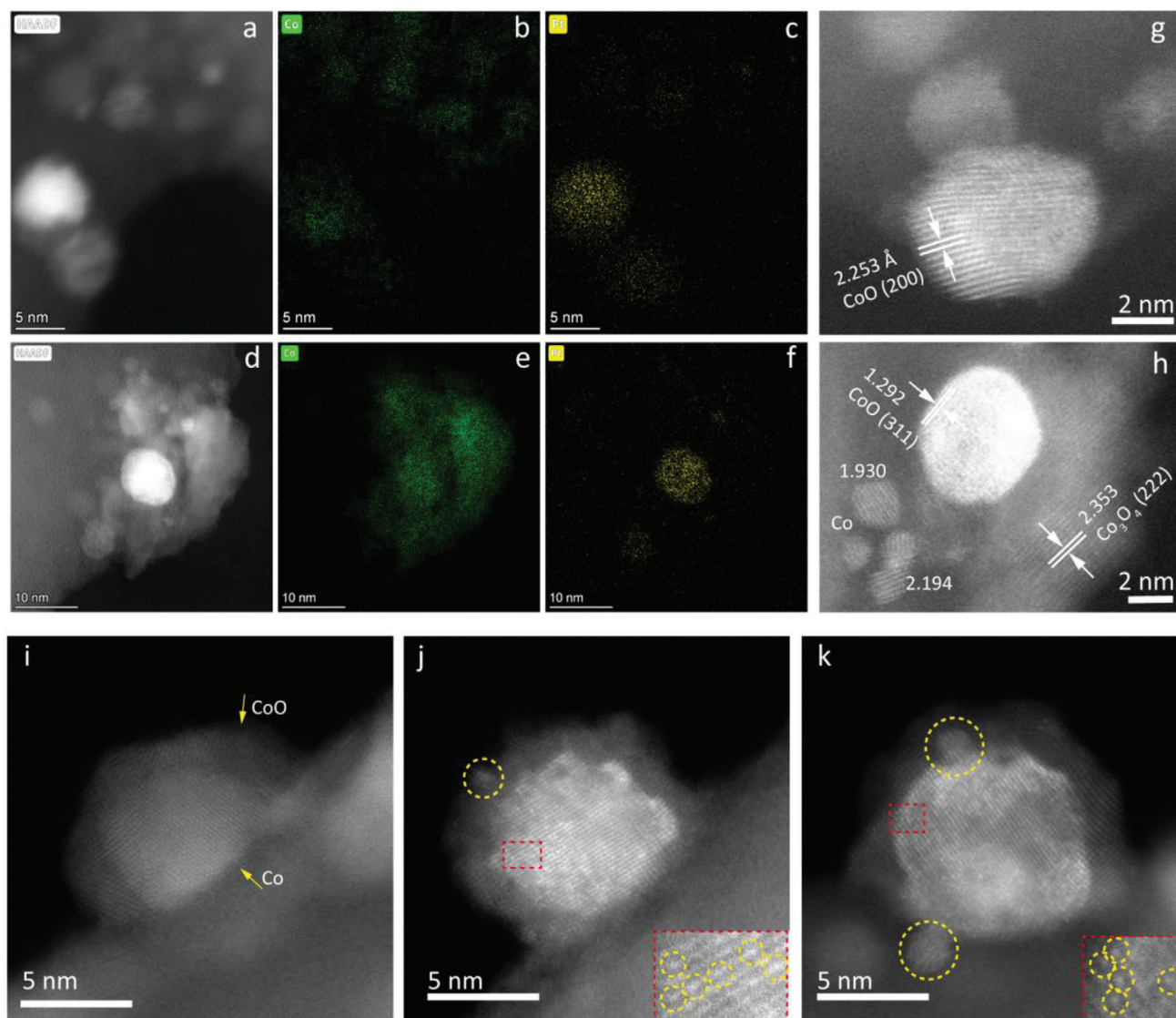The authors declare no conflict of interest.

Figure 7. Results of ex situ STEM studies. a–f) EDS elemental mapping of a–c) Pt-Co_3O_4-co and d–f) Pt-Co_3O_4-se precursors after in situ STEM reduction. g,h) Atomic resolution HAADF-STEM images of g) Pt-Co_3O_4-co and h) Pt-Co_3O_4-se after in situ reduction. i–k) Atomic resolution HAADF-STEM images of i) Co_3O_4, j) Pt-Co_3O_4-co, and k) Pt-Co_3O_4-se after ex situ reduction and passivation.

Data Availability Statement

The data that support the findings of this study are available from the corresponding author upon reasonable request.

Keywords

cobalt-based catalyst, cobalt oxide reduction, in situ ambient pressure transmission electron microscopy (TEM), Pt location and distribution, Pt promoting effect, temperature-programmed reduction

[1] P. Arnoldy, J. A. Moulijn, *J. Catal.* **1984**, *17*, 38.
[2] R. Bechara, D. Balloy, J.-Y. Dauphin, J. Grimblot, *Chem. Mater.* **1999**, *11*, 1703.
[3] D. I. Enache, B. Rebours, M. Roy-Auberger, R. Revel, *J. Catal.* **2002**, *205*, 346.
[4] A. Moen, D. G. Nicholson, B. S. Clausen, P. L. Hansen, A. Molenbroek, G. Steffensen, *Chem. Mater.* **1997**, *9*, 1241.
[5] A. M. Hilmen, D. Schanke, K. F. Hanssen, A. Holmen, *Appl. Catal., A* **1999**, *186*, 169.
[6] G. Jacobs, T. K. Das, Y. Zhang, J. Li, G. Racoillet, B. H. Davis, *Appl. Catal., A* **2002**, *233*, 263.
[7] A. Kogelbauer Jr., G. G. James, R. Oukaci, *J. Catal.* **1996**, *160*, 125.
[8] N. I. Il'chenko, *Russ. Chem. Rev.* **1972**, *41*, 47.
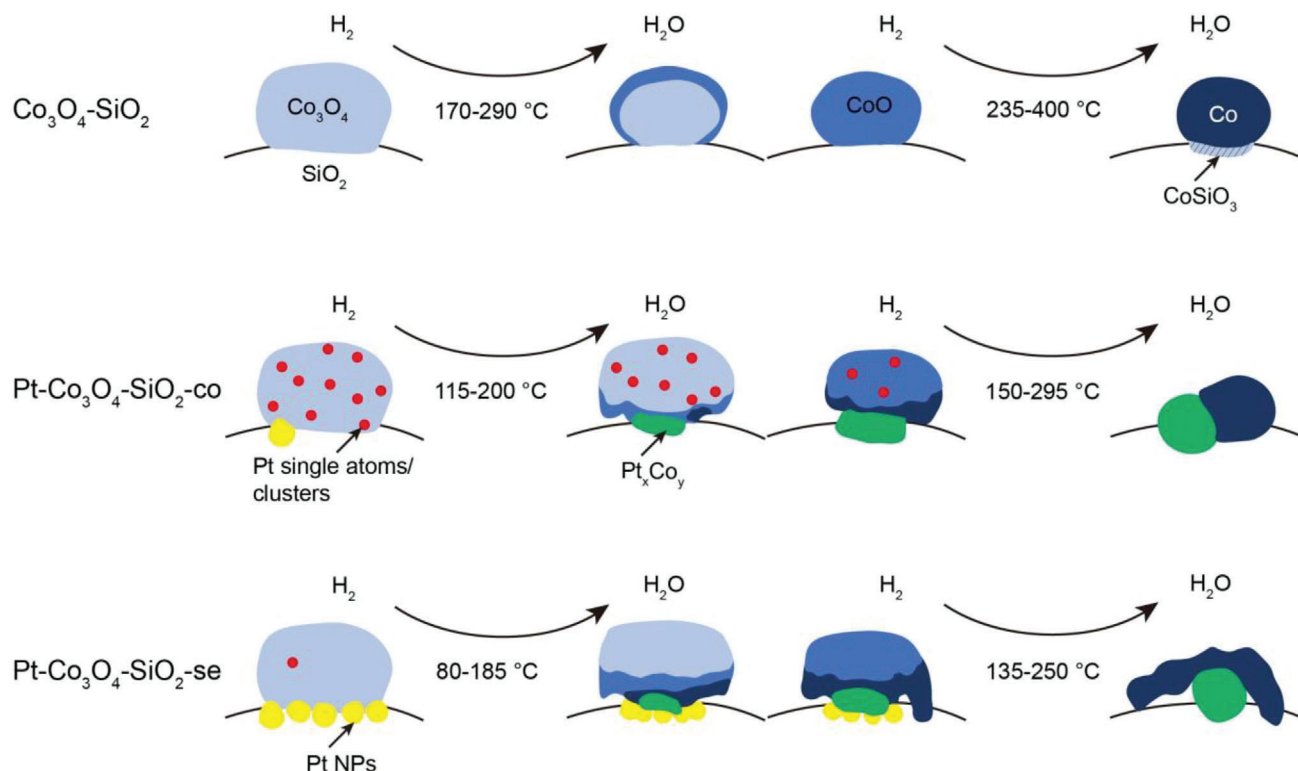[9] D. Xu, W. Li, H. Duan, Q. Ge, H. Xu, *Catal. Lett.* **2005**, *102*, 229.

ADVANCED
SCIENCE NEWS

www.advancedsciencenews.com

NANO · MICRO
small

www.small-journal.com

Figure 8. A model proposed for the effects of Pt promotion and its distribution on the reduction of silica-supported Co_3O_4 NPs.

[10] J. P. den Breejen, P. B. Radstake, G. L. Bezemer, J. H. Bitter, V. Frøseth, A. Holmen, K. P. de Jong, *J. Am. Chem. Soc.* **2009**, *131*, 7197.

[11] X. Sun, A. I. O. Suarez, M. Meijerink, T. van Deelen, S. Ould-Chikh, J. Zečević, K. P. de Jong, F. Kapteijn, J. Gascon, *Nat. Commun.* **2017**, *8*, 1680.

[12] T. M. Eggenhuisen, P. Munnik, H. Talsma, P. E. de Jongh, K. P. de Jong, *J. Catal.* **2013**, *297*, 306.

[13] L. Guczi, D. Bazin, I. Kovács, L. Borkó, Z. Schay, J. Lynch, P. Parent, C. Lafon, G. Stefler, Zs. Koppány, I. Sajó, *Top. Catal.* **2002**, *20*, 129.

[14] A. Y. Khodakov, W. Chu, P. Fongarland, *Chem. Rev.* **2007**, *107*, 1692.

[15] T. Jermwongratanachai, G. Jacobs, W. D. Shafer, V. R. R. Pendyala, W. Ma, M. K. Gnanamani, S. Hopps, G. A. Thomas, B. Kitiyanan, S. Khalid, B. H. Davis, *Catal. Today* **2014**, *228*, 15.

[16] N. Yamane, K. Suzuki, M. Tan, N. Tsubaki, *J. Jpn. Inst. Energy* **2017**, *96*, 250.

[17] T. O. Eschemann, J. Oenema, K. P. de Jong, *Catal. Today* **2016**, *261*, 60.

[18] J. H. den Otter, H. Yoshida, C. Ledesma, D. Chen, K. P. de Jong, *J. Catal.* **2016**, *340*, 270.

[19] D. Nabaho, W. J. (Hans) Niemantsverdriet, M. Claeys, E. van Steen, *Catal. Today.* **2016**, *261*, 17.

[20] G. Jacobs, J. A. Chaney, P. M. Patterson, T. K. Das, J. C. Maillot, B. H. Davis, *J. Synchrotron. Radiat.* **2004**, *11*, 414.

[21] M. Shannon, C. Lok, J. Casci, *J. Catal.* **2007**, *249*, 41.

[22] K. M. Cook, H. D. Perez, C. H. Bartholomew, W. C. Hecker, *Appl. Catal., A* **2014**, *482*, 275.

[23] M. Tang, W. Yuan, Y. Ou, G. Li, R. You, S. Li, H. Yang, Z. Zhang, Y. Wang, *ACS Catal.* **2020**, *10*, 14419.

[24] M. Tang, S. Li, S. Chen, Y. Ou, M. Hiroaki, W. Yuan, B. Zhu, H. Yang, Y. Gao, Z. Zhang, Y. Wang, *Angew. Chem., Int. Ed.* **2021**, *60*, 22339.

[25] W. Yuan, B. Zhu, X.-Y. Li, T. W. Hansen, Y. Ou, K. Fang, H. Yang, Z. Zhang, J. B. Wagner, Y. Gao, Y. Wang, *Science* **2020**, *367*, 428.

[26] W. Yuan, B. Zhu, K. Fang, X.-Y. Li, T. W. Hansen, Y. Ou, H. Yang, J. B. Wagner, Y. Gao, Y. Wang, Z. Zhang, *Science* **2021**, *371*, 517.

[27] H. L. Xin, E. A. Pach, R. E. Diaz, E. A. Stach, M. Salmeron, H. Zheng, *ACS Nano* **2012**, *6*, 4241.

[28] M. R. Ward, E. D. Boyes, P. L. Gai, *ChemCatChem* **2013**, *5*, 2655.

[29] M. R. Ward, E. D. Boyes, P. L. Gai, *J. Phys.: Conf. Ser.* **2014**, *522*, 012009.

[30] R. W. Mitchell, D. C. Lloyd, L. G. A. van de Water, P. R. Ellis, K. A. Metcalfe, C. Sibbald, L. H. Davies, D. I. Enache, G. J. Kelly, E. D. Boyes, P. L. Gai, *ACS Catal.* **2018**, *8*, 8816.

[31] K. Dembélé, M. Bahri, C. Hirlimann, S. Moldovan, A. Berliet, S. Maury, A.-S. Gay, O. Ersen, *ChemCatChem* **2021**, *13*, 1920.

[32] C. Ma, Y. Yun, T. Zhang, H. Suo, L. Yan, X. Shen, Y. Li, Y. Yang, *ChemCatChem* **2021**, *13*, 4350.

[33] A. Straß-Eifert, T. L. Sheppard, C. D. Damsgaard, J. Grunwaldt, R. Güttel, *ChemCatChem* **2021**, *13*, 718.

[34] R. Dehghan, T. W. Hansen, J. B. Wagner, A. Holmen, E. Rytter, Ø. Borg, J. C. Walmsley, *Catal. Lett.* **2011**, *141*, 754.

[35] E. van Steen, G. S. Sewell, R. A. Makhothe, C. Micklethwaite, H. Manstein, M. de Lange, C. T. O'Connor, *J. Catal.* **1996**, *162*, 220.